Research Article

DETERMINATION OF DIFFERENT OPTICAL PROPERTIES FOR CUBIC TITANIUM DIOXIDE: AN *AB-INITIO* APPROACH

Debashish Dash[1]*, Chandan K. Pandey[1], Saurabh Chaudhury[1], Susanta K. Tripathy[2]

[1] Department of Electrical Engineering, National Institute of Technology, Silchar, Assam, India

[2] Department of Electronics and Communication Engineering, National Institute of Technology, Silchar, Assam, India

* Corresponding author's e-mail: debashishdashnits@gmail.com

ABSTRACT

This paper presents an analysis of optical properties of cubic titanium dioxide (TiO_2) using Orthogonalized Linear Combinations of Atomic Orbitals (OLCAO) basis set under the framework of Density Functional Theory (DFT). Many optical properties such as refractive index, extinction coefficient, reflectivity, absorption coefficient, photoconductivity, and loss coefficient have been studied and analyzed thoroughly. From the analysis of optical properties, it is seen that, cubic TiO_2 supports interband transition between states. Reflectivity of pyrite structure TiO_2 lies within IR-visible – UV region due to which it qualifies for coating industry. Furthermore, the results are compared with previous theoretical as well as with experimental results. It is found that DFT based simulation produces results which are close approximation to experimental results.

Keywords: DFT, cubic TiO_2, refractive index, absorption coefficient, reflectivity

INTRODUCTION

Titanium Dioxide (TiO_2), is a material of interest for semiconductor industries due to its wide band gap property. In general, it is found naturally in different structures and crystalline forms like, monoclinic, orthorhombic, simple tetragonal, cubic [1]. It provides many intermediary utilization ways when it is grown in different polymorphic forms. Naturally, titanium dioxide forms in three different structures namely most stable rutile, medium stable anatase and less stable brookite [2]. Since last century, many types of advanced materials has been invented by applying high pressure on the crystal structure which may be significant for many electronic and industrial applications. Jin- Hua Wang *et al.* used the technique such as laser light excitation to investigate the Raman and photoluminescence spectra of a cubic structure named as yttrium oxide (Y_2O_3) [3]. Yugui *et al.* synthesized noble nitride material, under high pressure and high temperature [4]. Thus, it is clear that, high pressure plays an important role which transform a material to other form of material. Gong *et al.* [5] simulated many thermodynamic properties of an ideal glass and got concluded that, ideal glass manifest cooperative diffusion and clearly shows distinguished behaviour from the liquid state. They also clearly demonstrated that, glass state has flat potential landscape which was the most critical feature of ideal glass. So it is important to analyse the optical aspect of catalytic material like titanium dioxide. It is found that, if high pressure is applied to rutile type polymorphs, they get converted to fluorite type (CaF_2) and pyrite (FeS_2) structure. In past few years, titanium dioxide has been evolved as most promising photo catalysts due to its number of merits like eco- nontoxicity, cost-effectiveness, long term stability [6, 7]. TiO_2 materials mainly utilized in civil products such as interior decoration, personal hygiene and beautification until

in 1972 two scientists Fujishima and Honda [8] used firstly TiO_2 electrode to photocatalyze water splitting [9, 10]. Since then, many researches are being carried out to find out different applications of different polymorphs of titanium dioxide. Cubic TiO_2 has superb optical absorption transitions in the range of visible light (3.26 *eV* – 1.59 *eV*) due to which it is a best candidate material for making solar cells. Some distinguished industrial and commercial applications such as, transparent windows and glasses, highly efficient solar cells, dynamic random access modules, photodetectors and creating super hard materials, are distinctly encouraged in present era [11-13]. If it is in the powdered form, this can be used as pigment for painting as well as for making plastics. However, considering future conservation of energy and cleanliness of environment, solar cell is most important application for which cubic TiO_2 may be a preferred material [14-16]. So, for various monitoring or control applications, optical characterization is much necessary. Optical properties are unique in nature and easy to characterize any type of semiconductor material. Some optical properties can be (1) They can be adaptive with any type of environment including high-vaccume environment (2) They provide much necessary information which will be helpful for analyse transport properties of impurity or various defects and electrical behaviour. (3) They have abilities to provide analysis for long-range wave length/energy, finest results and high degree of accuracy by which it's possible for chemical and elemental analysis (4) Finally, these properties act as "table-top" properties for semiconductor manufacturing industry. In general, the cubic TiO_2 is synthesized from anatase TiO_2 by heating at a high temperature of 1900 to 2100 K in a diamond-anvil cell under a pressure of 48 GPa [17-19]. Investigation on both phases of cubic TiO_2 have been carried out by many research groups both experimentally and theoretically. Kim *et al.* [20] performed neutron scattering experiment and concluded that pyrite TiO_2 is unstable because of the imaginary frequencies in the phonon spectra during the entire pressure range, however fluorite TiO_2 is stable because of absence of such imaginary frequencies [20]. Imaginary frequency can be implied as a negative force constant i.e. in one direction energy is maximum whereas other orthogonal directions energy is minimum. Miloua *et al.* [6] studied both the cubical TiO_2 in detail using full potential linearized augmented plane wave method.

Moreover, Mattesini *et al.* [20, 21] found out that, the only difference between both the cubic phases of TiO_2 is the concern about positions of oxygen atoms located. In pyrite TiO_2, oxygen atoms are located at whereas in fluorite structure, these are at. Similarly, Zhao et al investigated different material parameters such as diffusion, interfacial energy using atomistic simulation. Following the same way, Hu *et al.* [22] concentrated the study on electronic and other properties using density functional theory and ultra-soft pseudopotentials. Previously, we have studied detailed analysis on structural, electronic and mechanical properties of both phases of cubic TiO_2 [23], but dielectric properties of both phases of cubic TiO_2 have not been studied.

From the literature, it is clear that, numerous investigations are being carried out for natural TiO_2. Most of the investigations of TiO_2 are on its structure, electronic and thermodynamic properties whereas very few investigations are carried out on dielectric properties of both phases cubic TiO_2. Hence, detailed investigation and analysis of structural and dielectric properties are motivated for various applications. In this paper, a systematic *ab-initio* investigation of the structural, and dielectric properties of cubic TiO_2 are studied in detail.

COMPUTATIONAL METHODS

Theoretical simulations were performed using orthogonalized linear combinations of atomic orbitals method. For titanium material, s and p local orbitals were added to the LCAO basis set for improving the convergence of considered wave function whereas for oxygen, a single orbital s were added to the basis set. All the LCAO parameters are optimized using Limited Memory Broyden - Fletcher - Goldfarb - Shanno (LBFGS) algorithm which is more popular compared to First Inertial Relaxation Engine (FIRE) and other Quasi Newton optimization algorithms. While simulating the default lattice parameters of both the crystals are varied within and then plotted the characteristic curve between total energy in Hartree (*Htr*) and total volume in Bohr. The relationship between these quantities is shown Figure 1a and 1b for fluorite and pyrite TiO_2 respectively**.** All the optimized lattice parameters and specifications are considered from [24]. The optimized fluorite and pyrite structure shown in Figure 2a and 2b respectively.
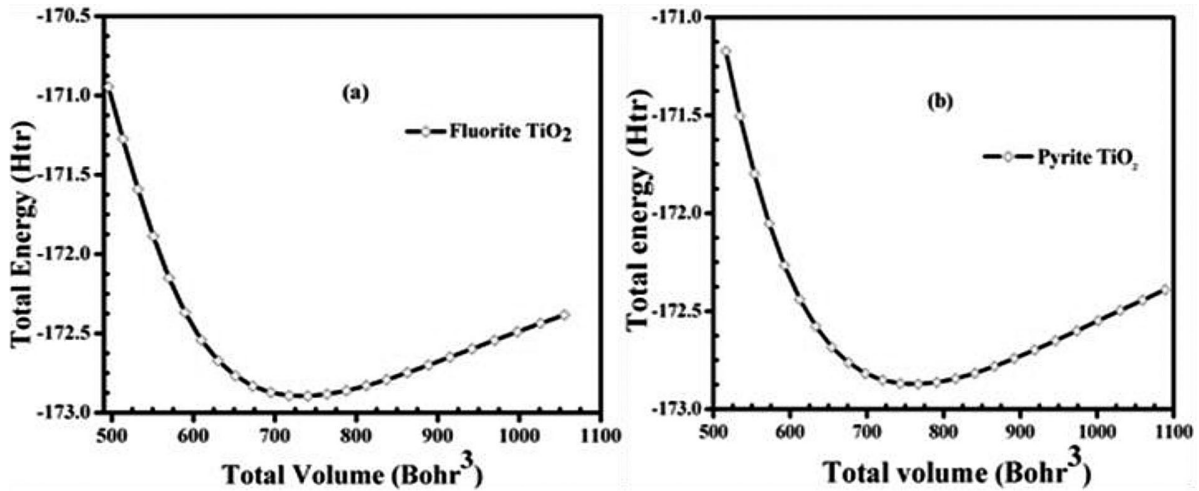
Fig. 1. (a) Total Energy vs Total Volume for fluorite type TiO_2 (b) Total Energy vs Total Volume for pyrite type TiO_2
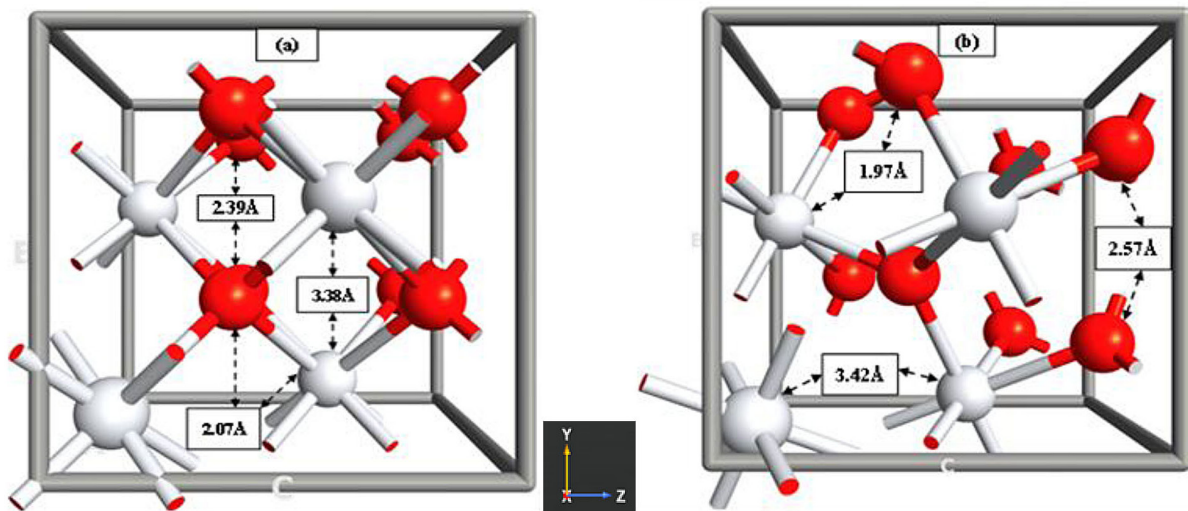

Fig. 2. (a) Optimized Fluorite TiO_2, (b) Optimized Pyrite TiO_2

Geometrical atom positions for fluorite structure: Titanium 4a (0, 0, 0) and Oxygen 8c (1/4, 1/4, 1/4). Similarly for pyrite structure: Titanium 4a (0, 0, 0) and Oxygen, 8c (x, x, x), x = 0.3411. The interatomic distance for each phase of cubic TiO_2 was shown in Figure 1 [24].

Big balls (white) represents Ti (Titanium) atoms and small balls (red) represents O (oxygen) atoms.

RESULTS AND DISCUSSION

With the density functional theory framework presented in the computational section, the simulation results and analysis on optical properties of fluorite and pyrite TiO_2 is shown here. This simulations are performed in a 12 GB Z380 HP workstation with 12 GB RAM using Virtual Nano Lab (*VNL*) software from Quantumwise Atomistix Tool Kit (*ATK*) [25-27].

Optical properties

For optical and opto-electronic applications, it is very crucial to understand and manipulate polarization of light. Many optical designs basically focus on wave length and intensity of light without concentrating on polarization. But polarization affects the laser beam focus, influences the cut-off wavelength of filters and most importantly to prevent unwanted back reflection. It is a known fact that, light is an electromagnetic (EM) wave, and the oscillations of the electric field is ⊥ to

the direction of propagation for which it need detailed analysis on each aspect of optical properties. Here, main focus is on the unpolarized light wave, as such the direction of this electric field varies randomly with time. The optical properties can be calculated considering real dielectric constant, $\varepsilon_1(\omega)$ and complex dielectric constant, $\varepsilon_2(\omega)$ using the following equation:

$$\varepsilon(\omega) = \varepsilon_1(\omega) + i\varepsilon_2(\omega) \qquad (1)$$

As TiO_2 is considered as a super-photo catalytic material, a detailed investigation is needed to know its future applications. This can be accomplished if study on the dielectric properties of it is carried out. As in Eq. (1), the imaginary part, that is the complex dielectric constant ε_2, consists of two parts: one due to intraband transition of the incident electromagnetic (EM) wave and the other due to interband transition of the incident EM wave. For metals, intraband transition was considered whereas interband transition is for semiconducting materials. Again, the interband transition is of two types, direct band and indirect band transitions. Due to little contribution towards dielectric function, indirect interband transitions can be neglected, although it provides information regarding electron-phonon scattering. The direct interband transitions contributes mainly to the dielectric function (imaginary part) which can be found out from the momentum matrix between occupied and unoccupied wave functions. For evaluating real and imaginary parts of the dielectric function, the Kubo-Greenwood formalism has been used [24, 28]. Mathematically, it can be expressed as:

$$\chi_{ij}(\omega) = -\frac{e^2\hbar^4}{m^2\varepsilon_0 V\omega^2}\sum_{nm}\frac{f(E_m)-f(E_n)}{E_{nm}-\hbar\omega-i\hbar\Gamma}\Pi^i_{nm}\Pi^i_{mn} \qquad (2)$$

Where Π^i_{nm} is the ith component of the dipole matrix element between state n and m, v is the volume, Γ is the broadening factor, and f the fermi function. The dielectric response co-efficients such as, the relative dielectric constant (ε_r), polarizability (α) and optical conductivity (σ) are related to susceptibility as:

$$\varepsilon_r(\omega) = (1+\chi(\omega)),$$
$$\alpha(\omega) = V_{\varepsilon_0}\chi(\omega),$$
$$\sigma(\omega) = -i\omega\varepsilon_0\chi(\omega) \qquad (3)$$

The fluorite and pyrite TiO_2 single crystals have a cubic symmetry, because of which they require only one dielectric tensor component to characterize the linear optical properties. For this reason, even if the linear dielectric tensor of both the crystals compounds have three independent components, but here one axis values have been considered to calculate different optical properties.

The imaginary part of the complex dielectric function as specified in Eq. (4), is obtained from the momentum matrix elements between the two electronic states that is occupied and unoccupied states. This can be expressed mathematically as,

$$\varepsilon_2(\omega) = \frac{2e^2\pi}{\Omega\varepsilon_0}\sum_{k,v,c}\left|\psi^c_k\left|u.r\right|\psi^v_k\right|^2\delta(E^c_k - E^v_k - E) \qquad (4)$$

Where ψ^c_k and ψ^v_k are the conduction band and valence band wave functions at k, u is the vector defining the polarization of the incident electric field, ω is the light frequency and e is the electronic charge. According to Kramers-Kronig transforms [29] the imaginary part given in Eq. (1) and calculates the real part of the dielectric constant. Mathematically, this can be expressed as,

$$\varepsilon_1(\omega) = 1 + \frac{2}{\pi}P\int_0^\infty\frac{\varepsilon_2(\omega)\omega'd\omega'}{\omega'^2 - \omega^2} \qquad (5)$$

In the above equation, P representing dominant value of integral.

Using the above dielectric constants Eq. (4) and (5), several optical properties such as refractive index (η), extinction co-efficient (k), reflectivity (r), absorption coefficient (α), photo-conductivity (σ), and loss coefficient (L) have been calculated.

The real part of dielectric function (ε_1) shows how much a material becomes polarized when an electric field is applied. This is due to creation of electric dipoles in the material. From Figure 2a, a major peak occurring at ~2 eV can be observed for the fluorite TiO_2. At this point, electron transition occurs at the Ti $3d$ states in the CB minimum to O $2p$ states in the VB maximum. The observed dielectric constant is 4.7 eV for fluorite type TiO_2 using the Perdew-Zunger exchange correlation parameters under the framework of LDA. Dielectric constant for different exchange correlation are shown in Table 1. Similarly, it can be seen that from Figure 3b for the pyrite TiO_2 real dielectric constant, it can be seen that, there is two peak points situated at ~1.8 eV and 2 eV. The first peak is weak and corresponds to the Ti $3p$ and O $2s$ states in the lower valence band whereas the second peak is the highest occurring point which is
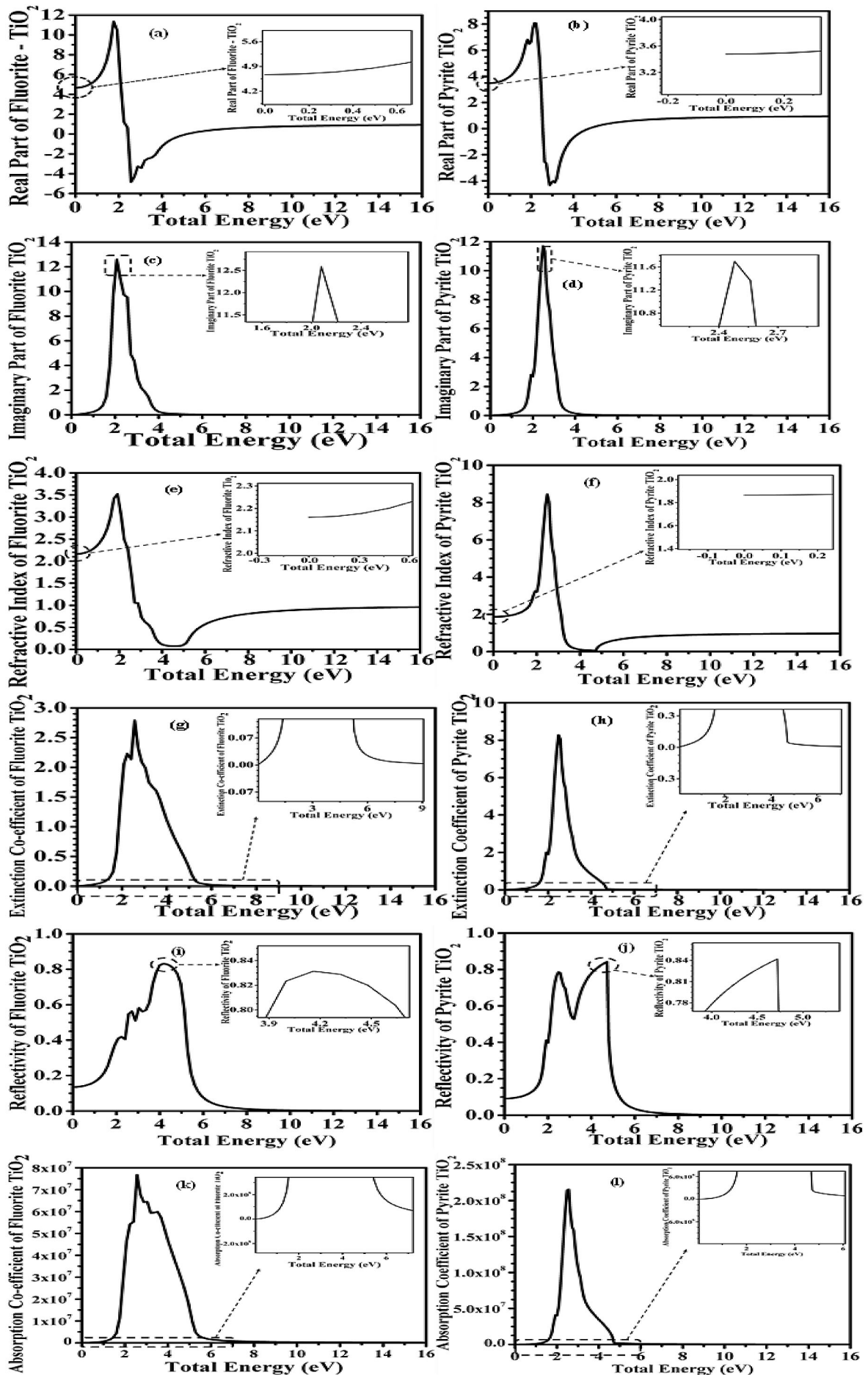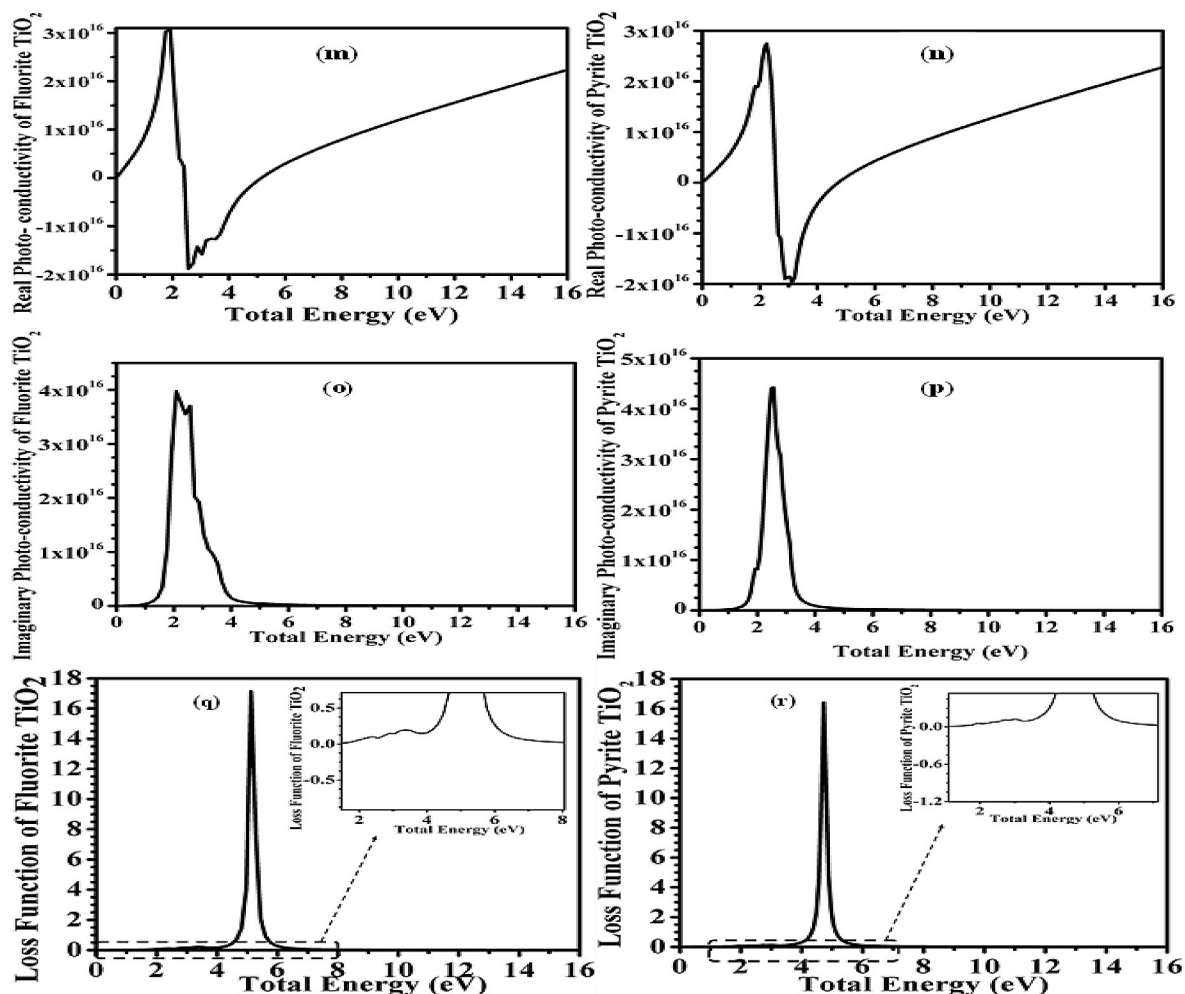
Fig. 3. (a) Real part of dielectric constant of fluorite TiO_2 (b) Real part of dielectric constant of pyrite TiO_2 (c) Imaginary part of dielectric constant of fluorite TiO_2 (d) Imaginary part of dielectric constant of pyrite TiO_2 (e) Refractive index of fluorite TiO_2 (f) Refractive index of pyrite TiO_2 (g) Extinction coefficient of fluorite TiO_2 (h) Extinction coefficient of pyrite TiO_2 (i) Reflectivity of fluorite TiO_2 (j) Reflectivity of pyrite TiO_2 (k) Absorption coefficient of fluorite TiO_2 (l) Absorption coefficient of pyrite TiO_2 (m) Real photo conductivity of fluorite TiO_2 (n) Real photo conductivity of pyrite TiO_2 (o) Imaginary photo conductivity of fluorite TiO_2 (p) Imaginary photo conductivity of pyrite TiO_2 (q) Energy Loss Function of fluorite TiO_2 (r) Energy Loss Function of pyrite TiO_2

caused due to transition of electron from conduction band minimum at Ti *3d* states and valence band maximum at O *2p* states. For pyrite, the observed dielectric constant is lower than fluorite structure having value of 3.5 *eV*.

The absorption property of any material can be known from the imaginary part of the dielectric constant as in Eq. (1). If this value is, then the material is transparent. When absorption begins, this value becomes non-zero. The peak absorption occurs at 2.1 *eV* which is due to direct interband transitions as well as direct excitons of the fluorite structured TiO_2 whereas for pyrite structured TiO_2, the peak occurs at 2.45 *eV*. The imaginary part of dielectric constant for both the structure shown in Figure 3c and 3d respectively.

The calculated values of dielectic constants as obtained from Eq. (2), (3), (4) and (5) also validate the equation for dielectric constant in terms of refraction [30] as given below:

$$\varepsilon = \eta^2 \qquad (6)$$

Where η is the index of refraction. It is a function of photon energy and it can be given as:

$$n = \eta + ik \qquad (7)$$

where: n – the complex refractive index,
$\quad \eta$ – the refractive index,
$\quad k$ – the extinction co- efficient.

When light passes through a material, it interacts with the constituent molecules or atoms. These interactions has a direct effect on the bend-

ing of light. As temperature increases, the interaction of molecules decreases. From *Fig. 3 (e) and (f)*, it can be seen that the calculated value of refractive index η is 2.16 for the fluorite TiO_2 and 1.9 for pyrite TiO_2 respectively. The refractive index for other type of exchange correlation methods given in Table 1. With lower refractive index, more and more light absorption takes place. Moreover, due to this light also travels faster. Because of these reasons, efficiency of solar energy conversion increases. So, pyrite type TiO_2 is much more efficient compared to fluorite type TiO_2. In this case, the fluorite structure will have more bending effect as compared to pyrite TiO_2, because it has more refractive index [31].

The extinction coefficient (k) for both the structures is displayed in Figure 3g and 3h. Basically, k indicates the amount of absorption loss when the electromagnetic wave propagates through the material. Normally, similar characteristics for (k) and absorption coefficient (α) can be observed. It is found from Figure 3g that, for fluorite type TiO_2, molar absorptivity starts from 0 eV and continues up to 9 eV. Thus in the energy range, 0 eV<$k \leq 9$ eV, fluorite type TiO_2 behaves as a transparent material. At 3 eV, rises to its global maximum value, and then gradually falls to its minimum value at around 9 eV. Similarly, for pyrite structured TiO_2, molar absorptivity starts from 0 eV and continues up to 7 eV. In the energy range, 0 eV<$k \leq 7$ eV, pyrite type TiO_2 behaves as a transparent material. At ~2.5 eV, rises to its global maximum value, and then gradually falls to its minimum value at around 7 eV as seen from Figure 3h.

Figure 3i and 3j shows the reflectivity curve of fluorite and pyrite structures of TiO_2. The term reflectivity means when a photon beam is bombarded with the material, some portion of the beam is reflected back or scattered at the interface between the two media even if both materials are transparent in nature. The reflectivity $R(\omega)$ of any material with normal light incidence can be calculated using refractive indices (η) and extinction coefficient (k) by the following Fresnel equation [32, 33]:

$$R(\omega) = \frac{(1-\eta)^2 + k^2}{(1+\eta)^2 + k^2} \qquad (8)$$

From Eq. (8), it can be observed that at lower energy, fluorite type TiO_2 shows strong reflectivity. For fluorite structure TiO_2, the global maximum occurs at 4.15 eV which arises due to interband transition. This global maxima occurs at an energy level within the Infrared and ultraviolet region, from which it can be inferred that, fluorite type TiO_2 can be best used as a coating material [34, 35]. After this, a sharp decrement can be seen which results in minimum reflectivity at energies in the range 6–9 eV, beyond which reflectivity is much lower and can be negligible. This minimized reflectivity is due to a collective plasma resonance. This plasma resonance can be determined by the imaginary part of dielectric constant which also represents the degree of overlapping between the inter-band absorption regions. When total energy increases towards higher range, fluorite material shows no reflectivity. Similarly, for pyrite structure TiO_2, a strong reflectivity can be observed in the energy range 0–5 eV. The maximum reflectivity also happens around 4.7 eV. Then reflectivity sharply decreases and comes to very low value at 9 eV. In pyrite type TiO_2 also reflectivity lies within IR-visible-UV region, due to which it is also suitable as coating material [34, 35].

The absorption coefficient (α) on the other hand, provides some important information regarding maximum solar energy conversion efficiency. It also describes, how far a light with a specific energy or wavelength can travel before being absorbed. Figure 3k and 3l shows absorption curve for fluorite and pyrite structure TiO_2. From the characteristics curves, it can be observed that for compound semiconductor material, like TiO_2, the absorption coefficient does not start from origin. This is due to non-metallic nature of the material. For fluorite type TiO_2, the absorption coefficient starts from 1 eV and rises up to a value at 7 eV approximately and then gradually decreases to a value at around 9.5 eV. Beyond 10 eV, no absorption happens as shown in Figure 3k. For the region 0-2 eV, the characteristics curve is known as fundamental absorption edge. The fluorite TiO_2 attains global maxima for absorption curve near to 3 eV which was formed due to valence to conduction band region popularly known as Interband Absorption Region (IAR). It can be observed that, there is a small edge near to 3.2 eV which occurs for free excitons and an edge near to 4 eV which occurred due to bounded excitons. As the main fact is, more the absorption value more is the electrons penetrated into TiO_2 by capturing large number of electrons that fall on it. So, for any semiconductor, it is advantageous to have more absorption coefficient. Similarly, for pyrite TiO_2, absorption starts from 0.6 eV up to a maximum value at 5.8 eV approximately and then

decreases gradually to a value near to 12 *eV* and after this, no absorption happens as shown in *Fig. 3 (l)*. For pyrite type TiO$_2$, valence to conduction band transition occurs near at 2.6 *eV*. Mathematically, the absorption coefficient can be calculated from the following expression,

$$\alpha = \frac{4\pi k}{\lambda} \qquad (9)$$

where: k – extinction coefficient, '

λ – the wavelength.

Figures 3(m-p) shows the real photo-conductivity of fluorite and pyrite type TiO$_2$. The main fact is, as large absorption amount at the surface of the material, more number of electrons released from the surface due to which electrical conduction can be expected from the surface of material when bombarded with photons. Similarly, in the case of semiconductor, when photons are bombarded with energy greater than the band gap energy, it may resulted in creation of electron-hole pairs. This process is called photo-conductivity. The current produced due to photo-conductivity is directly related to the incident light intensity. This property is very important in case of photovoltaic cell popularly known as solar cell which is used for conversion of solar energy to electricity. The conductivity for real part (σ_r) and imaginary part (σ_i) for the dielectric function $\varepsilon(\omega)$ are related through the expression [33] given below,

$$\sigma_r = \omega\varepsilon_1(\omega)$$

$$\sigma_i = \omega\varepsilon_2(\omega) \qquad (10)$$

From eq. (10), it can be observed that, conductivity is proportional to real and imaginary part of dielectric constant which is in good agreement with our results as shown in Figure 3(i-j) and Figure 3(k-l). The electrical conductivity of any medium increases, as it absorbs more and more photons. It can be seen that both fluorite and pyrite TiO$_2$ has good absorption values. So these two structures can provide good electrical conductivity.

Figure 3q and 3r shows the energy loss function (*ELF*) for fluorite and pyrite TiO$_2$. It explains, how much is the energy loss occurs when a fast electron traverse through the material. In quantum physics, it can be defined as the bulk plasma frequency ω_p, which occurs when the imaginary dielectric constant, $\varepsilon_2<1$ and real dielectric constant $\varepsilon_1=0$. The loss spectra is much weaker in the lower energy regime, however it becomes significant at around 4 *eV* and continues up to 8 *eV*.

The instant at which maximum loss occur is at around 5 *eV*, which corresponds to plasmon energy $\hbar\omega_p$ of the fluorite type TiO$_2$ semiconductor. The characteristics below 4 *eV* is due to interband transitions whereas, the peak in the characteristics plot is after 4 *eV* which corresponds to bulk plasmon peaks associated with collective charge excitons. Thus it can be said that, oscillations are formed due to valence electrons linked with plasmon oscillations. Similarly, for pyrite structure TiO$_2$, ELF becomes significant at around 2.1 *eV* and continues up to 6.5 *eV*. The instant at which maximum loss occur is at around 5 *eV*, which corresponds to plasmon energy $\hbar\omega_p$ of the pyrite TiO$_2$ semiconductor [36, 37]. Mathematically, ELF can be given as [32]:

$$ELF = lm\left(\frac{-1}{\varepsilon(\omega)}\right) \qquad (11)$$

CONCLUSIONS

A simulation based study is presented here on the structural as well as frequency dependent dielectric properties within the dipole approximation for fluorite and pyrite TiO$_2$ material using OLCAO basis sets under the framework of DFT. Most results are compared with previously calculated LDA works as well as plane wave results and found competitive results using the above specified basis set. The calculated lattice parameters of fluorite compound is in good agreement with experimental data with a deviation of less than and due to unavailability of experimental findings for pyrite type cubic TiO$_2$, theoretical study will be much more helpful in near future. Moreover, in this work, investigation on the dielectric properties with LDA found to be very much closer to other researchers calculated values. Some underestimated value for some of the dielectric properties can be observed because a single exchange – correlation potential is not continuous across the band gap. By following two individual ways, error can be made less. First one is to implement Green's function instead of density functional theory. The Green's function can help to study self-energy of quasi particles in a many particle system. The second way can be, applying of self-interaction correction (*SIC*). Here, self-interaction in the Hartree term is removed by an orbital-by-orbital correction to the exchange-correlation potential. From the results, it has been observed that the dielectric functions

Table 1. Dielectric constants of cubic TiO_2 using the OLCAO, and other exchange correlation methods used with LDA

Phase	Methods	a ($\mathring{A}$)	Vol. ($\mathring{A}^3$)	$\varepsilon_1(0)$	η	Reference
Fluorite $(Fm3m)$	**LDA-PZ-OLCAO**	**4.787**	**109.696**	**4.7**	**2.2**	**This Study**
	LDA - B3LYP	4.744	106.766	7.348	2.711	[12]
	LDA-CAPZ	4.739	106.429	7.75	2.78	[17]
	LDA- VASP	4.748	107.08			[17]
	LDA-CASTEP	4.749	107.104			[38]
	EXPERIMENTAL	4.87	115.500			[12]
Pyrite $(Pa\bar{3})$	**LDA-PZ-OLCAO**	**4.844**	**113.661**	**3.75**	**1.90**	**This study**
	LDA - B3LYP	4.744	106.766	7.345	2.710	[12]
	LDA-CAPZ	4.807	111.1	7.64	2.76	[17]
	LDA- VASP	4.821	112.10			[17]
	LDA- CASTEP	4.805	110.95			[17]
	LDA- LCAO	4.800	110.66			[18]

Note: Column 1 indicates different phases of cubic TiO_2, column 2 indicates specific method of simulation, column 3 indicates about optimized lattice constant 'a' in $\mathring{A}^3$, column 4 indicates optimized volume of lattice, column 5 indicates dielectric constant '$\varepsilon_1(0)$' of cubic TiO_2, column 6 indicates refractive index of material and finally last column indicates the referred article.

agree with experimental values in case of both the cubic -TiO_2 with a minimal error. These underestimation can be avoided if better optimization algorithms are used.

REFERENCES

1. Jian-Zhi Zhao, Wang Guang-Tao, Yong-Cheng Liang. Mechanical properties and electronic structure of cotunnite TiO_2. Chin. Phys. Lett., 25, 2008, 4356.

2. Landmann M., Rauls E. and Schmidt W.G. The electronic structure and optical response of rutile, anatase and brookite TiO_2. J. Phys.: Condens. Matter, 24, 2012, 195503.

3. Wang Jin-Hua, Li Ze-Peng, Liu Bo, Liu Bing-Bing. Local microstructural analysis for $Y_2O_3/Eu^{3+}/Mg^{2+}$ nanorods by Raman and photoluminescence spectra under high pressure. Chinese Phys. B, 26(2), 2017, 026101.

4. Fan Long by, Zhang Ping, Has Songyan, Wang Yuan Xu, Liu Ping day, Wang Wenkui, Yao Yugui. Recent studies on the crystal structure, electronic structure and mechanical properties of noble metal nitrides. Physics, 36, 2007, p. 03:0.

5. Sun Deyan, Shang Cheng, Liu Zhipan, Gong Xingao. Intrinsic Features of an Ideal Glass. Chin. Phys. Lett., 34(02), 2017, 026402.

6. Miloua R., Kebbab Z., Benramdane N., Khadraoui M., Chiker F. Ab initio prediction of elastic and thermal properties of cubic TiO_2. Comp. Mat. Sci., 50, 2011, 2142-2147.

7. Shougaijam Biraj, Ngangbam Chitralekha, Lenka Trupti Ranjan. Plasmon-Sensitized Optoelectronic Properties of Au Nanoparticle- Assisted Vertical Aligned TiO_2 Nanowires by GLAD Technique. IEEE Trans. on electron dev., 64(3), 2017, 1127-1133.

8. Fujishima A. and Honda K. Electrochemical photolysis of water at a semiconductor electrode. Nature, 238, 1972, 37-38.

9. Liu Yan, Li Zhe, Green Michael, Just Michael, Yang Li Yang, Chen Xiaobo. Titanium dioxide nanomaterials for photocatalysis. J. of Phys. D, 50, 2017, 193003.

10. Shougaijam Biraj, Ngangbam Chitralekha, Lenka Trupti Ranjan. Enhancement of Broad Light Detection Based on Annealed Al-NPs Assistaed TiO_2-NWs Deposited on p-Si by GLAD Technique. IEEE Trans. on Nanotechnol., 17(2), 2018, 285-292.

11. Zhou Xiang-Feng, Dong Xiao, Qian Guang- Rui, Zhang Lixin, Tian Yonjun, and Wang Hui- Tian. Unusual compression behaviour of TiO_2 polymorphs from first principles. Phys. Rev. B, 82, 2010, 060102.

12. Qi Jun Liu, Zhang Ning-Chao, Liu Fu-Sheng, and Liu Zheng-Tang. Structural, elastic, electronic and optical properties of various mineral phases of TiO_2 from first- principles calculations. Phys. Scr., 89, 2014, 047101.

13. Li Jyun-Yi, Chang Sheng-Po, Hsu Ming-Hung and Chang Shoon- Jinn. Influence of Annealing Ambience on TiO_2 Film Ultraviolet Photodetector. ECS J. Solid State Sci. Technol., 6(2), 2017, Q3056-Q3060.

14. Zhang Jinfeng, Zhou Peng, Liu Jianjun and Yu Jiaguo. New understanding of the difference of

photocatalytic activity among anatase, rutile and brookite TiO_2. Phys. Chem. Chem. Phys., 16, 2014, 20382-20386.

15. Shougaijam Biraj, Swain Raghunandan, Ngangbam Chitralekha, Lenka Trupti Ranjan. Enhanced photodetection by glancing angle deposited vertically aligned TiO_2 nanowires. IEEE Trans. on Nanotechnol., 15(3), 2016, 389-394.

16. Jin En Mei, Jeong Sang Mun, Kang Hee- Cheol and Gu Hal-Bon. Photovoltaic Effect of Metal-Doped TiO_2 Nanoparticles for Dye-Sentitized Solar Cells. J. Solid State Sci. Technol., 5, 2016, Q109-Q114.

17. Mahmood Tariq, Cao Chuanbao, Tahir Muhammad, Idrees Faryal, Ahmed Maqsood, Tanveer M., Imran Aslam, Zahid Usman, Ali Zulfiqar, Hussain Sajan. Electronic, elastic, acoustic and optical properties of cubic TiO_2: A DFT approach. Physica B, 420, 2015, 74-80.

18. Liang Yongcheng, Zhang Bin, and Zhao Jianzhi. Mechanical properties and structural identification of cubic TiO_2. Phys. Rev. B, 77, 2008, 094126.

19. Kong X. G., Yu Y., and Gao T. Electronic excitation energies in TiO_2 in the fluorite phase. Eur. Phys. J. B., 76 2010, 365.

20. Kim D. Y., Almeida J. S. de, Koci L., Ahuja R. Dynamical stability of the hardest known oxide and the cubic solar material: TiO_2. Appl. Phys. Lett., 90, 2007, 171903.

21. Mattesini M., Almeida J. S. de, Dubrovinsky L., Dubrovinskaia N., Johansson B., and Ahuja R. Cubic TiO_2 as a potential light absorber in solar-energy conversion. Phys. Rev. B, 70, 2004, 115101.

22. Mattesini M., Almeida J. S. de, Dubrovinsky L., Dubrovinskaia N., Johansson B., and Ahuja R. High-pressure and high-temprature synthesis of cubic TiO_2 polymorph. Phys. Rev. B, 70, 2004, 212101.

23. Hu Xue-Lan, Zhao Ruo-Xi, Luo Yang, Song Qing-Gong. Effect of P impurity on $NiAl\Sigma5$ grain boundary from first-principles study. Chin. Phys. B, 26, 2017, 023101.

24. Dash Debashish, Pandey Chandan K., Chaudhury Saurabh, Tripathy Susanta K. Structural, electronic, and mechanical properties of cubic TiO_2: A first-principles study. Chin. Phys. B, 27, 2018, 017102.

25. Atomistix ToolKit version 2014.3, QuantumWise A/S (www.quantumwise.com)

26. Brandbyge M., Mozos J.–L., Ordejón P., Taylor J., and Stokbro K. Density-functional method for nonequilibrium electron transport. Phys. Rev. B, 65, 2002, 165401.

27. Soler J.M., Artacho E., Gale J.D., García A., Junquera J., Ordejón P., and Sánchez-Portal D. The SIESTA method for ab-initio order- N materials simulation. J. Phys. Condens. Matter, 14, 2002, 2745.

28. Desjarlais M.P. Density functional calculations of the reflectivity of shocked xenon with ionization based gap corrections. Contrib. Plasma Phys., 45, 2005, 300-304.

29. Wooten F. Optical Properties of Solids. New York and London Academic Press, 1972.

30. Callister William D. Materials Science and Engineering – An introduction, sixth edition. John Wiley & Sons Inc. 2004.

31. Ralls K.M., Courtney T.H. and Wulff J. Introduction to Materials Science and Engineering. New York John Wiley & Sons Inc., 1976.

32. Materials Studio CASTEP Manual Accelrys, 2010, http://www.tcm.phy.cam.ac.uk/castep/documentation/WebHelp/CASTEP.html.

33. Zhao Cuihua, Huang Dewei, Chen Jianhua, Li Yuqiong, and Du Zheng. First- principle study for influence of an external electric field on the electronic structure and optical properties of TiO_2. RSC Adv., 6, 2016, 98908-98915.

34. D. Di Claudio, A.R. Phani, S. Santucci. Enhanced optical properties of sol-gel derived TiO_2 films using microwave irradiation. J. of opt. mat., 30, 2007, 279-284.

35. Maruszczyk A., Dudek A., Szala M. Research into Morphology and Properties of TiO_2 – NiAl Atmospheric Plasma Sprayed Coating. Adv. in Sci. and Technol. Res. J.,11(3), 2017, 204-210.

36. Saniz R., Ye L. H., Shishidou T., and Freeman A. J. Structural, electronic and optical properties of $NiAl_3$: First-principle calculations. Phys. Rev. B 74, 2006, 014209.

37. Marton L. Experiments on Low-Energy Electron Scattering and Energy Losses. Rev. Mod. Phys., 28, 1956, 172-183.

38. Kuo Ming-Yu, Chen Cheng-Lung, Hua Chih-Yu, Yang Hsiao-Ching, Shen Pouyan. Density Functional Theory Calculations of Dense TiO_2 polymorphs: Implication for visible-light-responsive photocatalysts. J. Phys. Chem. B 109, 2005, 8693.